

Loss of *carbohydrate sulfotransferase 6* function leads to macular corneal dystrophy phenotypes and skeletal defects in zebrafish

Merve Basol^{1,2}, Esra Ersoz-Gulseven¹, Helin Ozaktas^{1,2}, Sibel Kalyoncu¹ , Canan Asli Utine^{1,3} and Gulcin Cakan-Akdogan^{1,4} 

1 Izmir Biomedicine and Genome Center, Turkey

2 Izmir International Biomedicine and Genome Institute, Dokuz Eylül University, Izmir, Turkey

3 Department of Ophthalmology, Faculty of Medicine, Dokuz Eylül University, Izmir, Turkey

4 Department of Medical Biology, Faculty of Medicine, Dokuz Eylül University, Izmir, Turkey

Keywords

carbohydrate sulfotransferase 6;
CRISPR/Cas9; keratan sulfate proteoglycan;
macular corneal dystrophy; zebrafish

Correspondence

G. Cakan-Akdogan, Izmir Biomedicine and
Genome Center, Mithatpasa St. 58-Z,
Balçova 35340, Izmir, Turkey

Tel: +90 232 299 4142

E-mail: gulcin.cakan@ibg.edu.tr

Website: <https://www.ibg.edu.tr/research-programs/groups/cakan-lab/>

Merve Basol and Esra Ersoz-Gulseven
contributed equally to this article

(Received 25 March 2024, revised 14 July
2024, accepted 19 November 2024)

doi:10.1111/febs.17337

The *carbohydrate sulfotransferase 6* (*chst6*) gene is linked to macular corneal dystrophy (MCD), a rare disease that leads to bilateral blindness due to the accumulation of opaque aggregates in the corneal stroma. *chst6* encodes for a keratan sulfate proteoglycan (KSPG) specific sulfotransferase. MCD patients lose sulfated KSPGs (cKS) in the cornea and the serum. The significance of serum cKS loss has not been understood. Zebrafish cornea structure is similar to that of humans and it contains high levels of sulfated cKS in the stroma. Here, zebrafish *chst6* is shown to be expressed in the cornea and head structures of the embryos. An animal model of MCD is developed by generating *chst6* mutant animals with CRISPR/Cas9-mediated gene editing. The dramatic decrease in cKS epitopes in the mutants was shown with ELISA and immunofluorescence. Morphological defects or alterations of jaw cartilage were detected in a minor fraction of the mutant larvae. Loss of cKS epitopes and morphological defects was fully rescued with wild-type *chst6*. Mutant adult zebrafish displayed all clinical manifestations of MCD, while a fraction also displayed jaw and skeleton defects. Opaque accumulations formed in the eye, which were alcian blue positive. Loss of cKS in the corneal stroma and a decrease in corneal thickness were shown. Interestingly, alteration of transforming growth factor beta-induced (BIGH3) expression which was not described in patients was also observed. This is the first report of an MCD model in a genetically tractable organism, providing a preclinical model and insight into the importance of KSPG sulfation for proper skeletal morphogenesis.

Abbreviations

bp, basepair; BIGH3, transforming growth factor beta induced; Cas9, *CRISPR-associated protein 9*; cb, ceratobranchial; cds, coding sequence; ch, ceratohyal; *chst6*, *carbohydrate sulfotransferase 6*; cKS, corneal keratan sulfate; CRISPR, clustered regularly interspaced short palindromic repeats; dpf, days postfertilization; DSB, double strand break; ECM, extracellular matrix; ELISA, enzyme-linked immunosorbent assay; f, frameshift; GAA, glacial acetic acid; GAG, glycosaminoglycan; Gal-GlcNAc, galactose ($\beta 1 > 4$)-*N*-acetylated glucosamine; gen, generation; GlcNAc6-ST, *N*-acetylglucosamine-6-*O*-sulfotransferase; gRNA, guide RNA; hpf, hours postfertilization; KS, keratan sulfate; KSPG (s), keratan sulfate proteoglycan(s); M, molar; MCD, macular corneal dystrophy; mpf, months postfertilization; NBF, neutral buffered formalin; O/N, overnight; PAM, protospacer adjacent motif; PAPS, 3'-phospho-5'-adenylyl sulfate; PBS, phosphate buffered saline; pd, PAPS deletion; PFA, paraformaldehyde; pg, picogram; PG, proteoglycan; T7EI, T7 endonuclease I; wt, wild-type.

Introduction

The composition and organization of the extracellular matrix (ECM) in the corneal stroma is essential to its transparency [1]. The keratocytes are the main architects of this ECM. They produce proteoglycans (PGs) and collagens which form a perfectly aligned lattice that remains hydrated and transparent in homeostasis. PGs play a key role in the maintenance of the corneal transparency by interacting closely with collagen bundles in the eye and regulating their sizes and alignment [2,3]. PGs are complex molecules, which diversify the structure and roles of their core proteins by the type(s), number, linkage type, length, and sulfation of the glycosaminoglycan (GAG) side chains [4]. Keratan sulfates (KS) are highly sulfated glycosaminoglycans (GAGs) that contain long repeats of Galactose ($\beta 1 > 4$)-*N*-Acetylated Glucosamine (Gal-GlcNAc) disaccharide repeats. They are found in keratan sulfate proteoglycans (KSPGs) such as lumican, keratocan, and in some complex proteoglycans such as aggrecan that carry more than one type of GAG [5]. The importance of keratan sulfates and their sulfation status in the cornea extracellular matrix are exemplified by diseases cornea plana type 2 and macular corneal dystrophy (MCD) that are linked to mutations in *keratocan* and *carbohydrate sulfotransferase 6* (*chst6*), respectively [6,7]. Macular corneal dystrophy is characterized by opaque aggregates that begin to accumulate in the cornea in early teen years and gradually increase to finally cause bilateral vision loss by the 4th decade of life which is treated with corneal transplantation [8]. Lack of preclinical *in vivo* models is a limitation for development and testing of treatment strategies.

Macular corneal dystrophy is caused by mutations in *chst6* gene which encodes for a *N*-acetylglucosamine-6-*O*-sulfotransferase (GlcNAc6-ST), the major enzyme for sulfation of KSPGs (MIM #217800) [9]. Lack of sulfated corneal keratan sulfate (cKS) in corneal stroma is common for MCD type I and type II, whereas MCD type I patients also lack cKS in serum [10,11]. Since the amount of cartilage proteoglycans is considered to be more than 100-fold of corneal KSPGs, serum cKS sulfate is considered to be a result of cartilage KSPG breakdown [12]. The cKS quantitation is done with an antibody that recognizes fully sulfated Gal-GlcNAc epitopes; therefore, the type of the PG is not defined; however, aggrecan is the most abundant cartilage PG that carries KS [13]. Although MCD type I patients were reported to lack sulfated KSPGs in the cartilage, no clinical symptoms in cartilage were reported to date [12,14].

Corneal KSPGs are in contact with collagen fibrils, and abnormalities in bundle sizes and organization of collagen fibrils are detected in MCD patient samples [2,15,16]. The

negative charge of the sulfate groups is proposed to be important for the hydration of the corneal ECM and collagen bundle size control by physical force [3]. Although an *in vitro* model via inhibition of sulfotransferases in cultured goat primary corneal cells was proposed, lack of ECM containing collagen bundles and PGs that are tightly organized is a major limitation of this 2D model [17]. Experimental demonstration of the disease mechanisms is yet to be done, since there are no *in vivo* disease models available. In humans, highly similar *chst5* and *chst6* genes encode for intestinal and corneal specific GlcNAc6-ST enzymes, respectively. On the other hand, mice have only *chst5* as the ortholog of these two genes. It was not possible to mimic MCD in mice although null mutants of *chst5* were generated [18], which may be explained by the fact that mouse cornea contains predominantly chondroitin sulfate PGs, whereas 80% of human corneal PGs are KSPGs [18]. Zebrafish has a *chst6* gene and it is in a unique position to model MCD, since the structure of the cornea is well conserved. Zebrafish corneal stroma is composed of keratocytes and precisely organized collagen lattices [19,20]. Importantly, 80% of the PGs in the zebrafish cornea are KSPGs [21]. Moreover, in zebrafish the main corneal KSPGs, *lumican* and *keratocan*, are conserved and stromal localization of cKS is detected as of larval stages [19,22,23].

No previous study described expression and function of *chst6* in zebrafish, while expression of *chst6* in embryonic zebrafish is reported in ZFIN [24]. Expression of the fully sulfated KSPGs in the Meckel's cartilage and ceratohyal cartilage was shown in 4-day-old zebrafish, suggesting that CHST6 may be functional in the cartilage tissue as well [25]. Here, loss-of-function *chst6* mutant zebrafish lines were generated, and the gene-phenotype relationship in macular corneal dystrophy was demonstrated [26]. Systemic effects of *chst6* mutation were demonstrated. A small fraction of mutants developed early morphological defects, jaw or skeleton deformations in larval or adult stages. The *chst6* mutant zebrafish were shown to develop macular corneal dystrophy symptoms at macroscopic, molecular, and histopathological levels.

Results

Carbohydrate sulfotransferase 6 expression during development

Whole mount *in situ* hybridization revealed that *chst6* is expressed in head structures and the trunk, at 24 and 30 h postfertilization (hpf). At 60–72 hpf, *chst6*

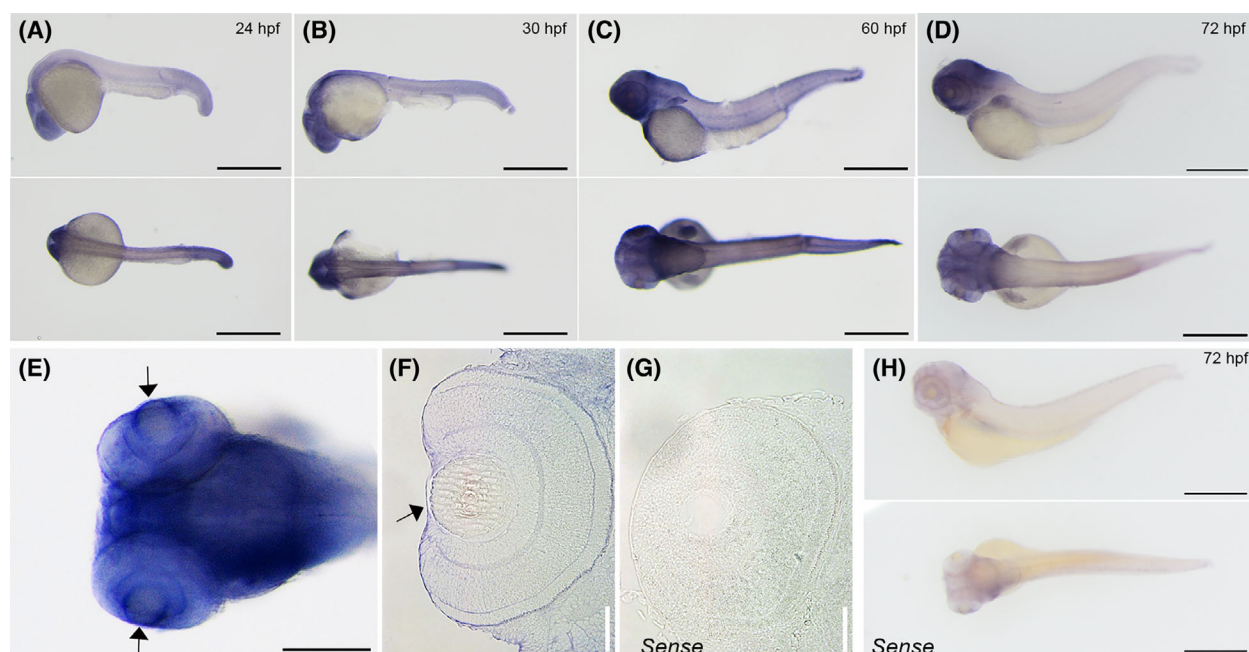


Fig. 1. The expression pattern of *chst6* in zebrafish embryos. Whole mount *in situ* hybridization revealed expression of *chst6* in the body of (A) 24 hpf, (B) 30 hpf, (C) 60 hpf, and (D) 72 hpf zebrafish. (E) Close-up image of the 72 hpf larval head shows strong expression in the brain and eye (arrow). The experiment was repeated three times and $n = 15$ for each stage. (F) Section of larvae post-*in situ* hybridization shows *chst6* expression in the cornea (arrow); (G) larvae stained with negative control sense probe did not show any signal in the eye. (H) Representative images of 72 hpf larvae stained with *chst6* sense probe (negative control). Scale bars: 100 μm .

expression becomes enhanced in the anterior tissues including the brain, eye, and jaw. At this stage, corneal layers are formed in the zebrafish eye [19]. Close-up images show strong *chst6* expression in the eye, and sections of the stained sample show expression in the retina and cornea of the larval eye (Fig. 1).

Zebrafish *chst6* mutants were generated via CRISPR/Cas9-mediated gene editing

In MCD patients, over one hundred variants of the *chst6* gene were reported. These mutations are distributed to the entire coding sequence of *chst6*, without any definite hotspot [27]. To choose the best target for CAS9, the structure of the CHST6 protein (Uniprot ID: Q9GZX3) was homology-modeled via SWISS-MODEL by using the crystal structure of *Mycobacterium avium* sulfotransferase protein (PDB ID: 2Z6V) as a template. The protein has a transmembrane domain (6–26) that ensures Golgi localization and a luminal sulfotransferase domain (27–395) (Fig. 2A). To predict the enzyme active site, the homology-modeled structure was analyzed by the PYMOL software (Schrodinger LLC, New York, USA). It was found that the 1st and 2nd 3'-phospho-5'-adenylyl sulfate (PAPS) binding sites form a sulfate passageway in the folded enzyme, while the arginine

in the 1st PAPS binding region (WRS₄GSSSF) was found to bind the SO₄ donor, suggesting it is the enzyme active site (Fig. 2B). This site is fully conserved among several vertebrate species including the zebrafish, and all residues but the first W are found to be mutated in patients [27]. Based on this knowledge, deletion or inactivation of 1st PAPS site was chosen as a strategy to generate *chst6* mutants. Guide RNAs (gRNAs) were designed with CRISPRscan to induce (a) a 50 bp deletion spanning the 1st PAPS site, (b) a double strand break (DSB) before the 1st PAPS binding site, (c) an early double strand break, and (d) deletion of the coding sequence (Fig. 2C) [28].

gRNA1 and gRNA2, that are predicted to target base pairs coding for 42 and 58 residues, respectively, were designed for deleting the 1st PAPS region. Resulted deletion mutations were identified by gel mobility shift of a PCR product that amplified 522 bp genomic DNA covering the target sites (Fig. 2A,D). The indel mutations induced with use of gRNA1 alone were detected with a T7 Endonuclease I mismatch assay (Fig. 2A,E). Although the highest scoring gRNA (gRNA5) targeted the 5th residue, no mutant alleles were obtained with this gRNA. Only one founder fish was obtained when gRNA5 and gRNA3 were used together, despite several trials. The targeted deletion

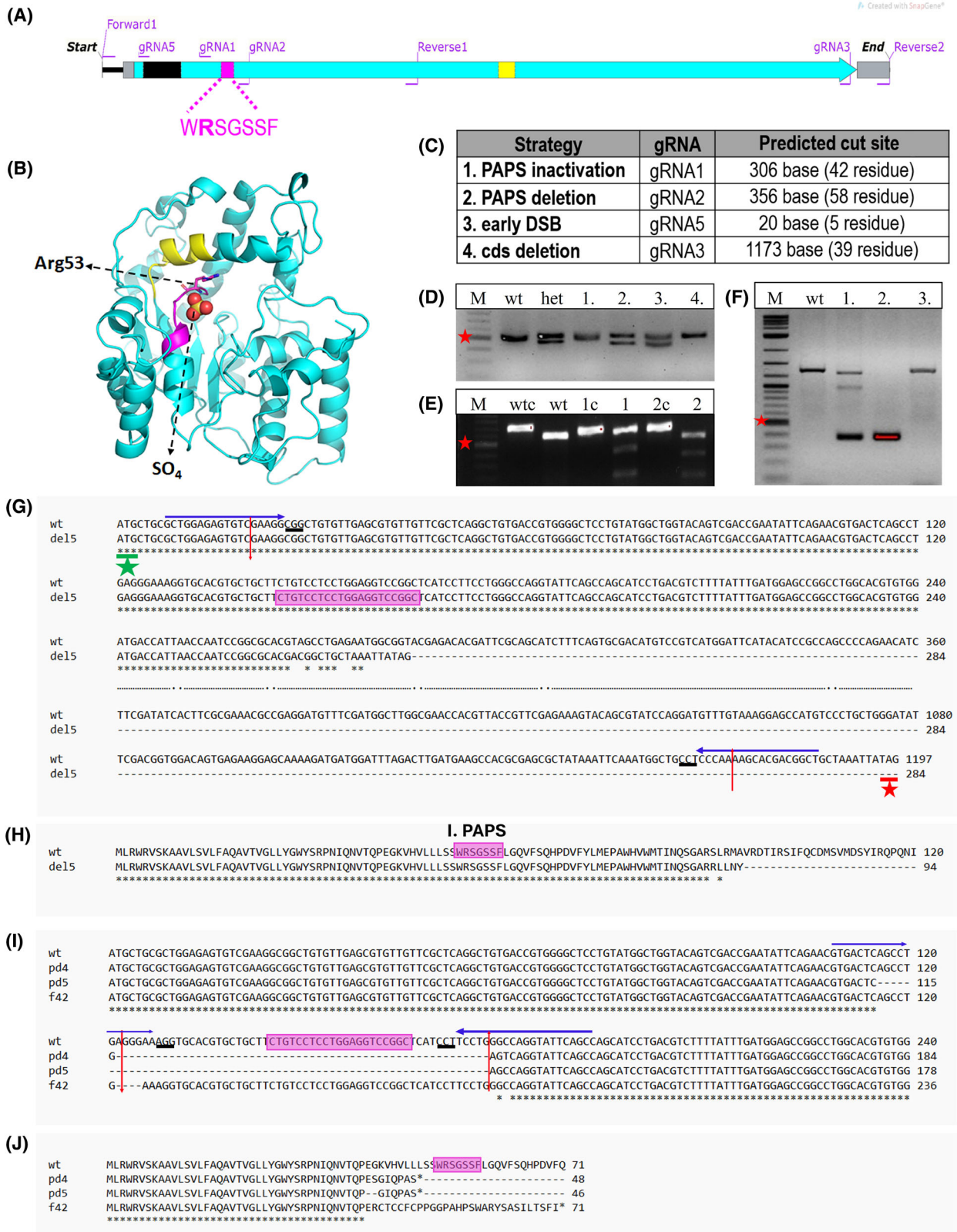


Fig. 2. *chst6* mutagenesis strategy. (A) Graphical representation of *chst6* gene cds. Carbohydrate sulfotransferase domain (turquoise), 1st PAPS (magenta), and 2nd PAPS (yellow) and transmembrane (black) domains are colored. Primers used for generating the PCR product for genotyping of PAPS domain mutants (forward 1, reverse 1); cds deletion mutant or Sanger sequencing (forward 1, reverse 2); and gRNA binding sites are indicated. (B) Model of zebrafish CHST6 sulfotransferase domain indicating localization of 1st PAPS (a.a. 49–55, magenta) and 2nd PAPS (a.a. 202–210, yellow) and SO₄ interaction with Arg53. Model was generated with the PYMOL Software. (C) Mutagenesis strategies and used gRNA annotations are shown. gRNA1 was used for the inactivation of the 1st PAPS domain by indel generation, gRNA1 and gRNA2 were used together to induce deletion of the 1st PAPS domain, gRNA5 was used to induce early indel before the transmembrane domain, and gRNA3 and gRNA5 were used together to induce deletion of the coding sequence. (D–F) Representative agarose gel images of genotyping analyses; (D) PAPS deletion (pd) mutation leads to generation of a 50 bp shorter mutant fragment. Lanes: marker, wt, heterozygous mutant, test fish 1, 2, 3, and 4 PCR products, (E) gRNA1 induced indel/frameshift (f) mutations were detected with T7E1 assay. Presence of mutant DNA strand leads to formation of a mismatch and digestion by T7E1. Lanes: marker, wt control, wt digested, fish 1 control, fish 1 digested, fish 2 control, fish 2 digested PCR products. (F) F₁ embryos obtained from founder fish of the cds deletion (del5) mutation were genotyped with PCR. *chst6* genomic region was amplified with forward 1 and reverse 2 primers. Heterozygous embryo 1 had 3 bands (wt, mutant, and heteroduplex), whereas embryo 2 had only the short band, and nonmutant embryo 3 had the wt DNA band. Short band was expected to be 150–160 bp, but a longer band was detected. Red asterisk shows 500 bp marker band in all gels. (G–J) Sequence alignments of obtained mutants with wt *chst6* (NM_001130621) were generated with CLUSTAL OMEGA web tool. gRNA binding sequences are indicated with arrows on top, predicted DSB site is indicated with red vertical arrow, 1st PAPS coding sequence is highlighted with magenta, PAM sequence is underlined, and start codon is indicated with a green asterisk. (G) DNA sequence, (H) protein sequence alignment of del5 mutant to wt, multiple sequence alignment of (I) DNA sequence, (J) protein sequence of homozygous mutants (*chst6*^{pd4/pd4}, *chst6*^{pd5/pd5}, and *chst6*^{f42/f42}) with wt.

was screened by PCR of the entire coding sequence (cds), and a 150–160 bp DNA band was expected; however, the detected band was larger (Fig. 2F). DNA sequence analysis revealed that a 943 bp deletion occurred in the *chst6* gene, and deletion started at 284th bp, 250 bp downstream of the predicted gRNA5 cut site leaving the 1. PAPS domain intact (Fig. 2G, H). Attempts to obtain homozygous adults failed and it was not possible to establish a mutant fish stock. Use of gRNA1 and gRNA2 together or gRNA1 alone both resulted in successful mutagenesis of the targeted regions, leading to generation of 6 and 13 founder fish, carrying PAPS deletion (pd) or indel frameshift (f) mutations, respectively. Sanger sequencing showed that pd4 and pd5 alleles have deletions very close to the predicted DSB sites (Fig. 2I). The calculated protein sequences showed that the deletion resulted in frameshift and truncation of the protein prior to 1st PAPS domain (Fig. 2J). Among the frameshift mutants, f42 has 6 nucleotide deletion at the gRNA1 predicted cut site and this caused a frameshift prior to the 1st PAPS domain and truncation at 71 residues. These three mutant alleles were further characterized.

Low penetrance developmental defects were observed in *chst6* mutant zebrafish

Mutant larvae displayed morphological defects at low penetrance, which were fully rescued by wt mRNA injection (Fig. 3A,B). Morphology of embryos obtained from *chst6*^{pd4/pd4} homozygous parents is reported in Fig. 3. Majority of embryos displayed normal morphology, 33% had mild bending at the anterior end of the

tail, 16% had severe defects including bending of the anterior trunk; hearth and yolk edema at 2 days postfertilization (dpf), and these phenotypes became more severe at 5 dpf. At 5 dpf, the severely affected larvae were nearly lethal with prominent edema in heart and yolk, underdeveloped head, and grossly curved trunk. The morphological defects were fully rescued when wt *chst6* mRNA was injected to 1-cell stage embryo, with 100% of the mutants showing normal morphology at 2 and 5 dpf. Similar phenotypes were observed in all three alleles. Since the larvae with severe defects did not survive, the larvae with normal or mild morphology were raised. Lethality was observed in the larval-to-juvenile stages; however, it was less pronounced in the next generations. To understand the penetrance of the phenotype, the morphology analysis was repeated in the progeny of homozygous mutants *chst6*^{pd4/pd4}, *chst6*^{pd5/pd5}, and *chst6*^{f42/f42} at different generations. Occurrence ratio of severe and mild body deformations varied across tested alleles and generations (Fig. 3C–E). Interestingly, a decrease in the penetrance was observed in more recently acquired generations (Fig. 3C–E). It is important to note that the developmental defects are seen in the progeny of adults with normal morphology.

To check whether the penetrance is higher when heterozygous parents were used, the survival rates of previously reared stocks were analyzed (Table 1). Twenty-four out of 50 *chst6*^{pd5/pd5} larvae obtained from heterozygous F₁ parents (stock03) died before reaching adulthood, and only 3 of the survivors were homozygous. On the other hand, only 2 out of 75 larvae died before reaching adulthood when the heterozygous parents of a later generation (stock40) were

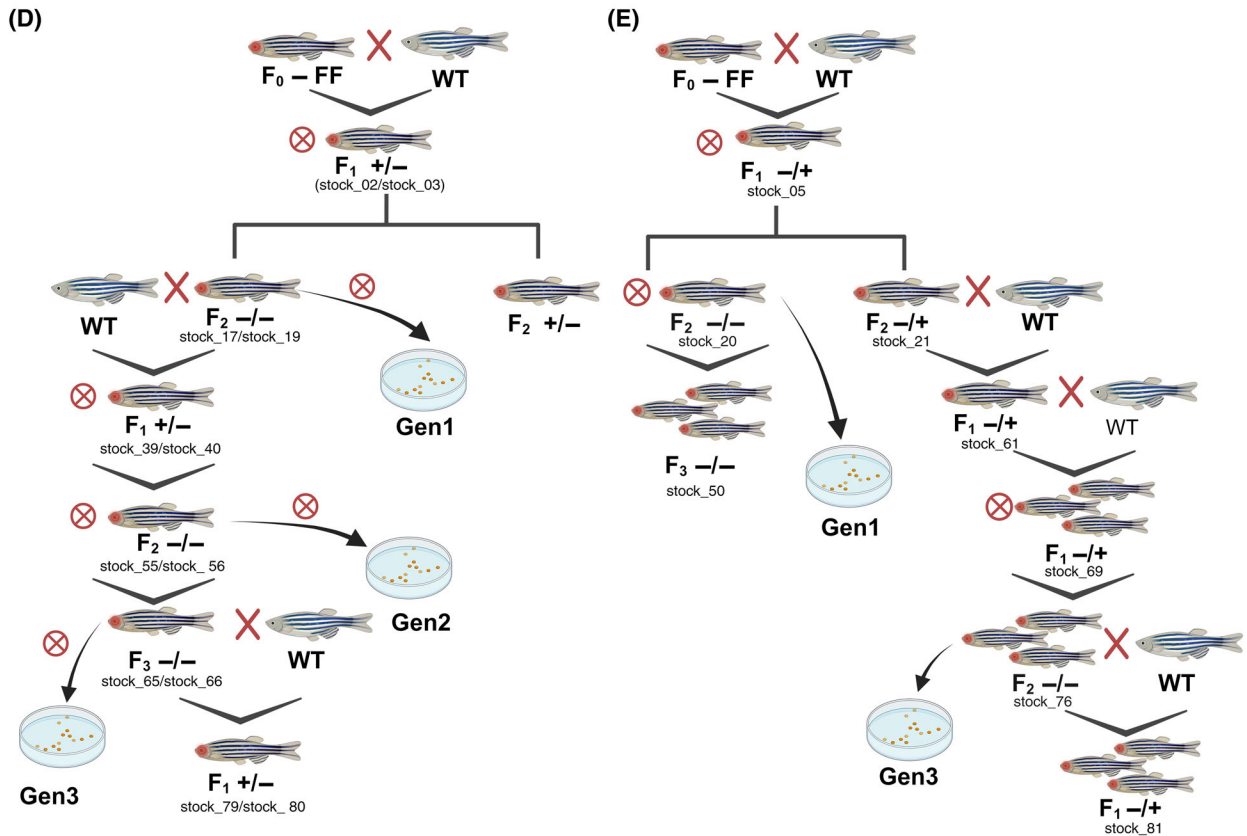
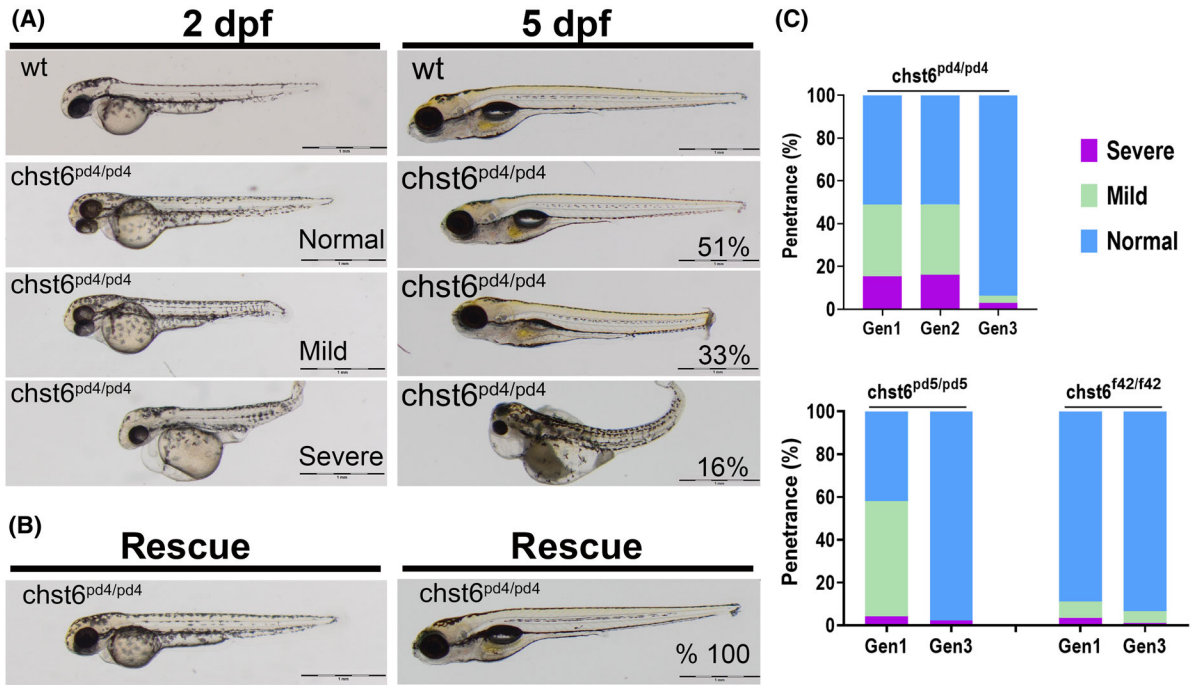


Fig. 3. Low penetrance morphological defects were observed in the mutant embryos. (A, B) Morphology of the wt, mutant, and mRNA-injected mutant embryos was analyzed at 2 and 5 dpf. Scale bars: 1 mm. (A) While majority of embryos displayed normal morphology, 33% had mild bending at the anterior end of the tail, 16% had severe defects including bending of the anterior trunk, hearth, and yolk edema at 2 dpf (left), and these phenotypes became more severe at 5 dpf (right) and they were nearly lethal with prominent edema in heart and yolk, underdeveloped head, and grossly curved trunk ($n = 113$). (B) The morphological defects were fully rescued when wt *chst6* mRNA was injected to 1-cell stage embryo, with 100% of the mutants has normal morphology at 2 and 5 dpf ($n = 68$). (C) Penetrance of morphological defect phenotype was analyzed at different generation in all three alleles, and ratios are shown in graphs. The defects were observed in < 5% of the mutants in generation (gen)2 and gen3 ($n = 54, 84$ and 226 for gen1, gen2, and gen3 of *chst6*^{pd4/pd4}, $n = 119$ and 44 for gen1 and gen3 of *chst6*^{pd5/pd5}, $n = 290$ and 84 for gen1 and gen3 of *chst6*^{f42/f42}, respectively). The breeding schemes for zebrafish mutant lines are illustrated in (D) for *chst6*^{pd4/pd4} and *chst6*^{pd5/pd5}, (E) for *chst6*^{f42/f42} mutant lines. Generations depicted in graphs (in C) are defined in the crossing schemes. Circled cross indicates inbreeding. D and E were created with BioRender.com

Table 1. Survival analysis of progeny obtained from heterozygous breeders.

No.	Genotype of parents	Stock no. of parents	No. of larvae at 6 dpf	No. of adult fish at 3 months	No. of homozygous fish
1	<i>chst6</i> ^{pd5/+}	Stock03	50	26	3
2	<i>chst6</i> ^{pd5/+}	Stock40	75	73	20
3	<i>chst6</i> ^{f42/+}	Stock05	50	36	10
4	<i>chst6</i> ^{f42/+}	Stock69	50	43	11

crossed, and 20 of these adults (stock56) were homozygous (Table 1, Fig. 3D). Similarly, 14 out of 50 *chst6*^{f42/f42} larvae obtained from heterozygous F₁ parents (stock05) died before reaching adulthood and 10 of these adults (stock20) were homozygous (Table 1, Fig. 3E). When the heterozygous parents of a later generation *chst6*^{f42/f42} (stock69) were incrossed, 7 out of 50 fish died before reaching adulthood and 11 adults (stock76) were homozygous (Table 1, Fig. 3E). Next, currently available heterozygous stocks were crossed in large numbers to assess the occurrence of severe phenotypes (Table 2, Fig. 3D,E). The latest generation of *chst6*^{pd4/pd4} (stock79) or *chst6*^{pd5/pd5} (stock80) yielded 6 (out of 669) and 3 (out of 990) severe embryos when incrossed, respectively (Table 2, Fig. 3D). When embryos of two different heterozygous generations, stock61 and stock81, were compared side by side, 3 (out of 145) and 3 (out of 1080) embryos displayed severe phenotype (Table 2). In summary, a decrease in the penetrance was also observed when heterozygous breeders were used. All of the following experiments were conducted with animals from at least two different generations.

The zebrafish *chst6* mutants lost sulfated keratan sulfates

In order to test for loss of function in the mutants, the 5D4 cKS antibody which recognizes the fully sulfated

Table 2. Embryo morphology analysis of progeny obtained from heterozygous breeders.

No.	Genotype of parents	Stock no. of parents	No. of larvae 5 dpf	No. of larvae with severe morphology
1	<i>chst6</i> ^{pd4/+}	Stock79	669	6
2	<i>chst6</i> ^{pd5/+}	Stock80	997	3
3	<i>chst6</i> ^{f42/+}	Stock61	145	3
4	<i>chst6</i> ^{f42/+}	Stock81	1080	3

Gal-GlcNAc epitopes of keratan sulfate was used [19]. Immunofluorescence staining showed that cKS signal is lost in the head of the mutants (Fig. 4A–C). The loss of cKS was a full penetrance phenotype in all generations and alleles of the *chst6* mutant zebrafish. Enzyme-linked immunosorbent assay (ELISA) was used to quantify cKS in the whole-body larval lysates. The total amount of cKS per larva was 65.7 picogram (pg) in wt larvae, while it was 15.4, 17.7, and 25.9 pg per *chst6*^{pd4/pd4}, *chst6*^{pd5/pd5}, and *chst6*^{f42/f42} larvae, respectively (Fig. 4D). Corneal cKS was detected in the eye of 4 dpf wt larvae, but cKS was not present in the eyes of any of the mutant lines (Fig. 4E–G). Loss of cKS in the cornea was rescued when wt *chst6* mRNA was injected into the zygotes of homozygous mutants (Fig. 4H).

Loss of CHST6 function led to skeletal defects in some zebrafish

The effects of cKS loss in cartilage and jaw cartilage of zebrafish larvae were investigated by alcian blue staining. The chondrocyte stacking and shape of cartilage tissue was normal; however, mutants displayed an increase of the angle at the joint that connects two ceratohyal cartilage (Fig. 5A–C). The distance between Meckel's cartilage and ceratohyal joint was increased in some mutants at 8 dpf, and both

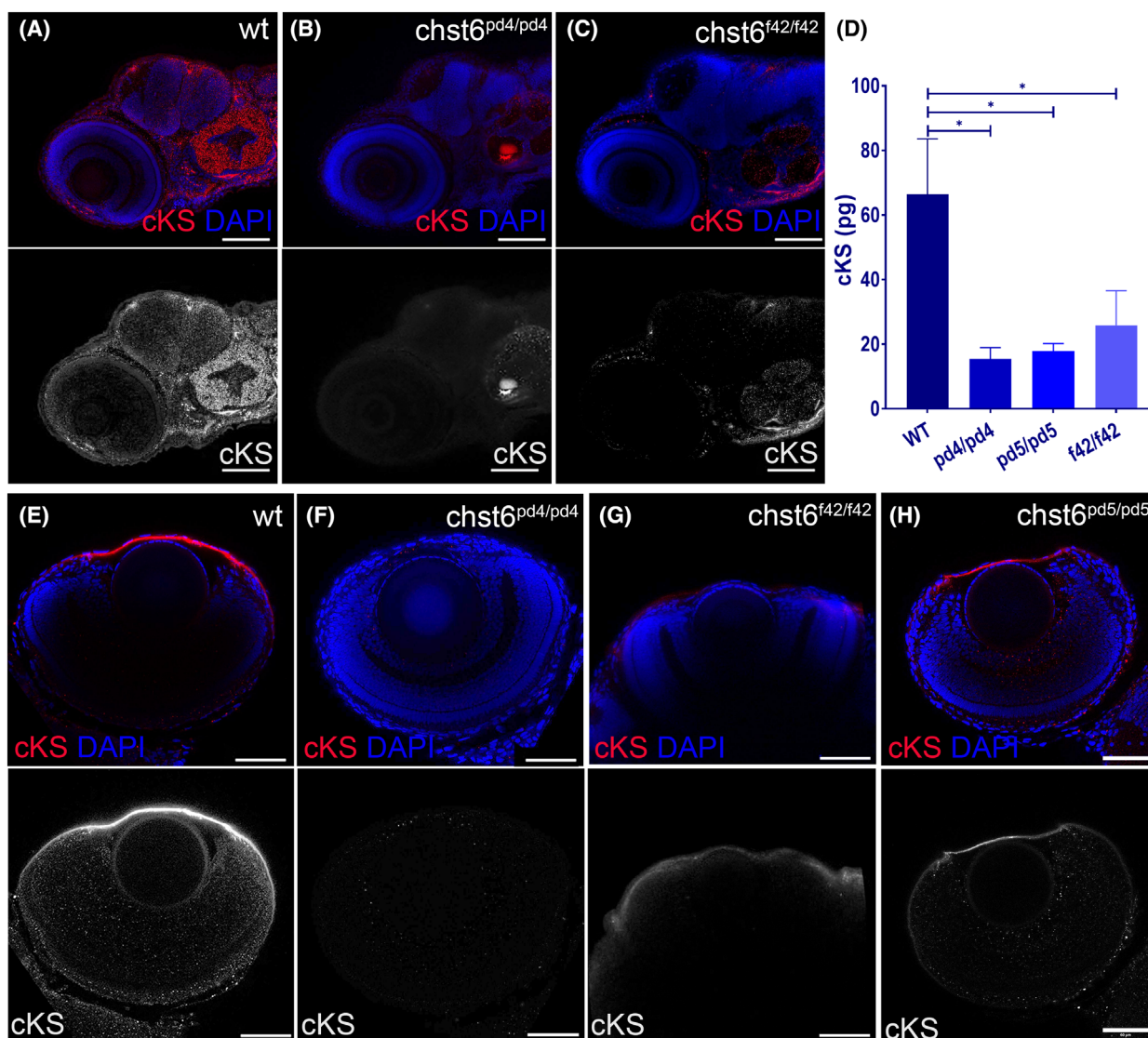


Fig. 4. *chst6* loss-of-function mutant phenotypes are rescued with wt mRNA. Loss of function was tested with cKS antibody using immunofluorescence and ELISA. (A) cKS epitopes are detected in the brain and otic vesicle of wt larvae at 4 dpf. The cKS signal is decreased in (B) *chst6*^{pd4/pd4} (C) *chst6*^{f42/f42} mutant larvae. (D) Total cKS in larval whole-body extracts were measured and displayed in the graph, and mean ± std values are wt: 66.36 ± 24.30 pg, *chst6*^{pd4/pd4}: 15.46 ± 6 pg, *chst6*^{pd5/pd5}: 17.83 ± 4.09 pg, *chst6*^{f42/f42}: 25.81 ± 18.59 pg ($n = 50$, 3 replicates for each group, one-way ANOVA was used for statistical analysis). Corneal cKS signal is detected in wt (E). Lost in all mutants (F) *chst6*^{pd4/pd4}, (G) *chst6*^{f42/f42} eye IF stainings are shown as examples. (H) cKS staining is rescued when wt mRNA is injected into 1-cell stage mutant embryos. $P < 0.05$ (*) Scale bars: 60 μ m.

phenotypes were most enhanced in the mutant larvae carrying the f42 allele of *chst6* (Fig. 5D). The plots show that some mutants diverge from the median considerably. Similarly, when the fish reached adulthood, only some of the *chst6* mutants had abnormal jaw appearance. Interestingly, *chst6*^{f42/f42} homozygous fish had a protruding mouth phenotype, whereas others had an open mouth phenotype (Fig. 5E).

Next, we analyzed the shape of trunks and the skeletal structure in adult mutants (Fig. 5F,G). As stated above, only the larvae with severe morphology did not survive beyond 5 dpf; therefore, normal looking or mildly affected larvae were raised. Most mutants developed to have normally shaped trunks. However, several fish with misshaped posterior were observed with bent spine, narrow posterior end caudal fin, or

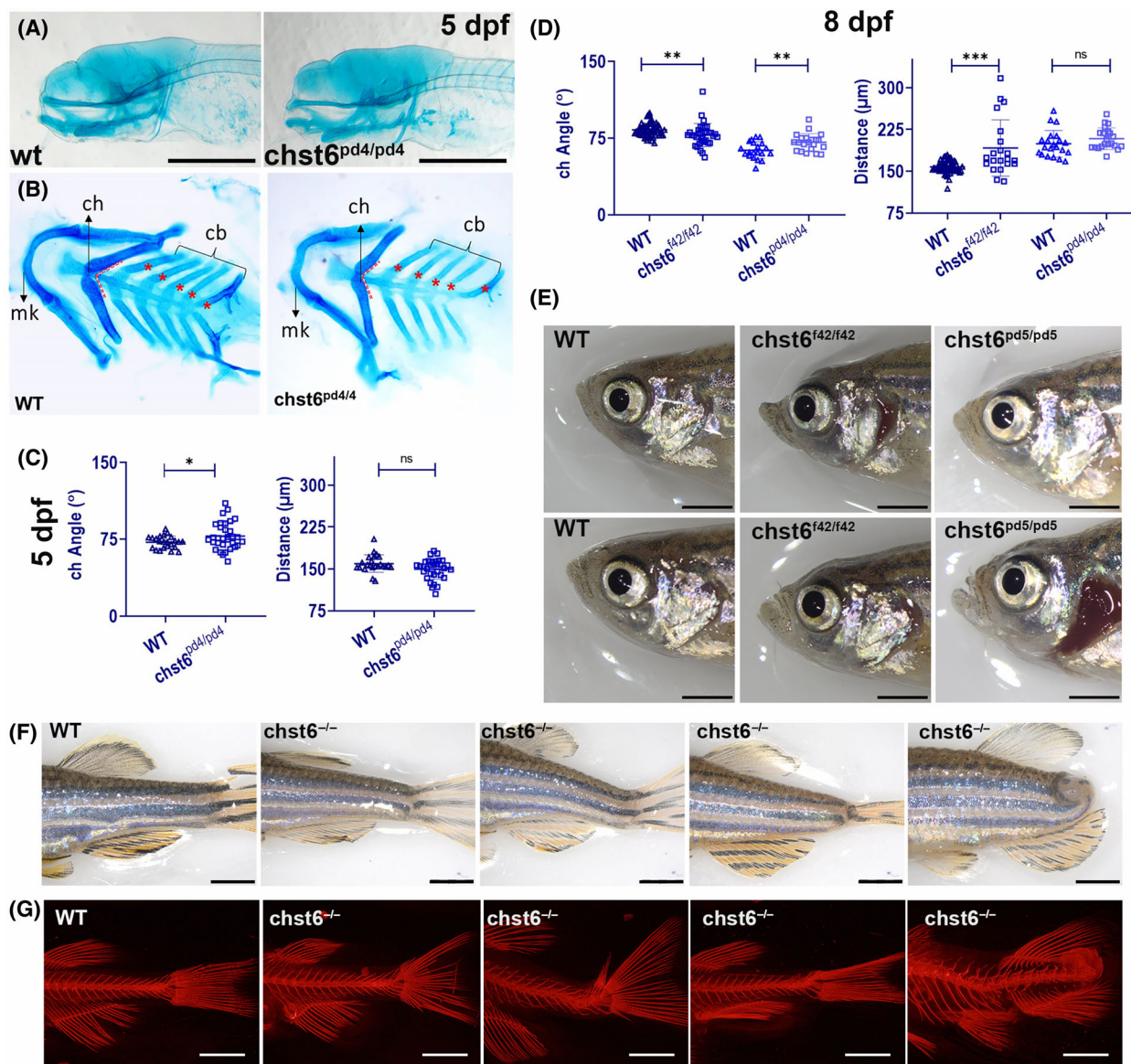


Fig. 5. Skeletal defects in *chst6* mutant zebrafish. (A–D) Alcian blue staining reveals defect in the lower jaw cartilage. (A) Lateral view, (B) dissected lower jaw of wt and *chst6*^{pd4/pd4} larvae. cb, ceratobranchial cartilage; ch, ceratohyal; mk, Meckel's cartilage; red dashed lines: the connecting angle of ch cartilages. (C, D) Graphs showing the angle between the mk and ch joints of (C) wt ($n = 23$) and *chst6*^{pd4/pd4} ($n = 32$) 5 dpf larvae; $P = 0.0494$ (angle), $P = 0.1444$ (distance), (D) wt ($n = 37$) and *chst6*^{f42/f42} ($n = 34$); wt ($n = 21$), and *chst6*^{pd4/pd4} ($n = 21$) 8 dpf larvae. $P = 0.0013$ (angle, wt vs *chst6*^{f42/f42}). $P = 0.0053$ (angle, wt vs *chst6*^{pd4/pd4}). $P < 0.001$ (distance, wt vs *chst6*^{f42/f42}). $P = 0.1789$ (distance, wt vs *chst6*^{pd4/pd4}). Multiple t -test was used for statistical analysis, nonsignificant (ns), $P < 0.05$ (*), $P < 0.01$ (**), $P < 0.001$ (***)). (E) Representative images of adult zebrafish with different face morphologies. (F) Representative images of adult zebrafish with different trunk phenotypes. (G) Alizarin red staining showing representative images of various skeletal phenotypes observed in mutant zebrafish. Scale bars: 300 μm (A), 2 mm (E, F). Images shown in E–G are representative images from different alleles. No correlation between certain phenotypes and alleles was observed.

no caudal fin at all (Fig. 5F). These differences were reflected also in the skeletal structure as revealed by alizarin red staining of the bone (Fig. 5G). The jaw and skeletal defects were rare but observed in different generations tested.

Macular corneal dystrophy symptoms were reproduced in zebrafish *chst6* mutants

Opaque aggregates were detected in mutants (Fig. 6). This phenotype was seen earliest at 8 months

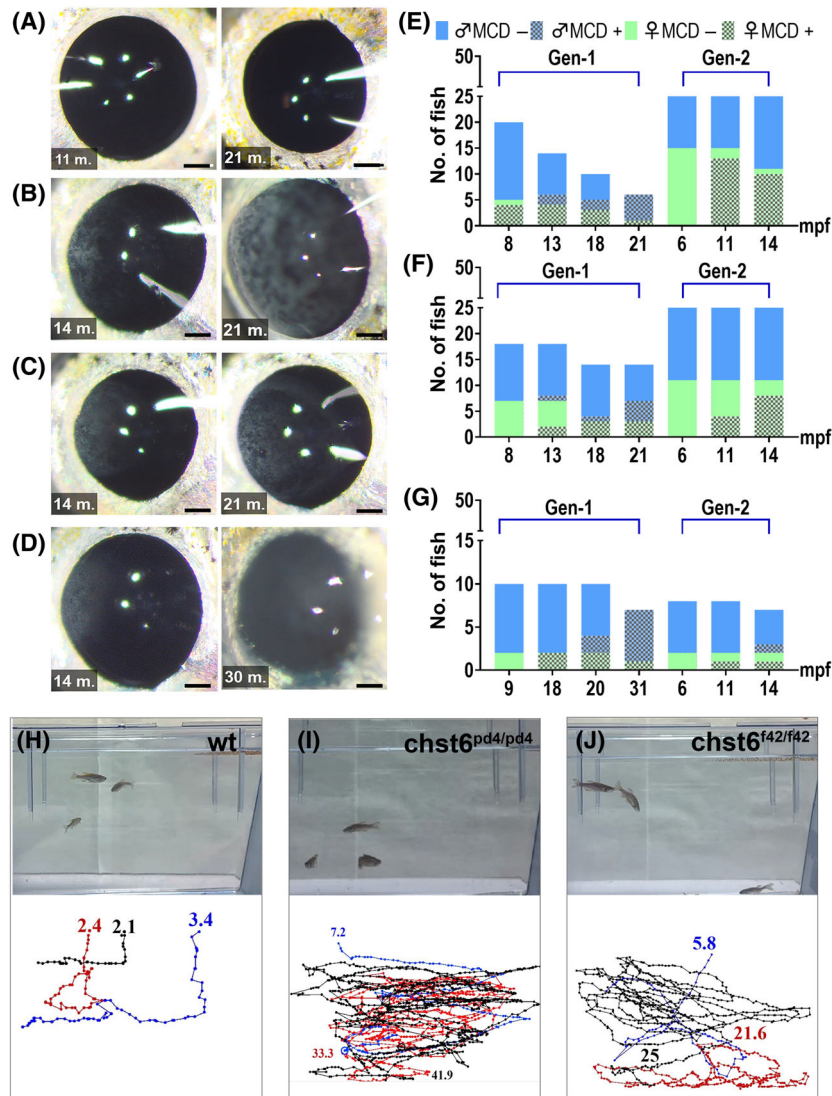


Fig. 6. *chst6* mutant zebrafish develop MCD and impaired vision. Macroscopic analysis of (A) wt, (B) *chst6*^{pd4/pd4}, (C) *chst6*^{pd5/pd5}, and (D) *chst6*^{f42/f42} alleles. Eyes of young (11–14 mpf) adults of gen2 (left), old (21–30 mpf) adults of gen1 (right) are shown. Scale bar: 300 μ m. (E–G) Incidence of opaque corneal aggregates homozygous mutants of two generations over time (E) Green bar: females, blue bar: males, dashed bars indicate occurrence of opaque aggregates. (E) *chst6*^{pd4/pd4}, (F) *chst6*^{pd5/pd5}, and (G) *chst6*^{f42/f42}. (H–J) The vision test was performed with wt and homozygous *chst6* mutants. Swim paths and durations were tracked. Track was ended if the fish reached food and time stamp is displayed at the end of each track. (H) wt fish swam for 2.4 and 3.4 s until it reached the food ($n = 3$). (I) *chst6*^{pd4/pd4} swam for 33.3 and 41.9 s without noticing the food ($n = 3$). (J) *chst6*^{f42/f42} swam for 21.6 and 25 s without noticing the food ($n = 3$).

postfertilization (mpf), the incidence of MCD phenotype increased over time, and most homozygous mutants developed opaque deposits between the ages of 14–20 mpf (Fig. 6A–D). The opaque eye phenotype was tracked in all three alleles in two generations and this phenotype was consistent, regardless of the general morphology of the fish (Fig. 6E–G). These aggregates impaired vision which was demonstrated by a reduced

response of mutant fish to food, dispersed on the surface of water (Fig. 6H–J, Videos S1–S3).

Paraffin sections of adult fish were stained with alcian blue and periodic acid Schiff. In the cornea of wt zebrafish, the epithelium was stained strongly positive with alcian blue, while some positive foci were detected in the stroma (Fig. 7A). The stroma of mutants was compact, and blue deposits were detected

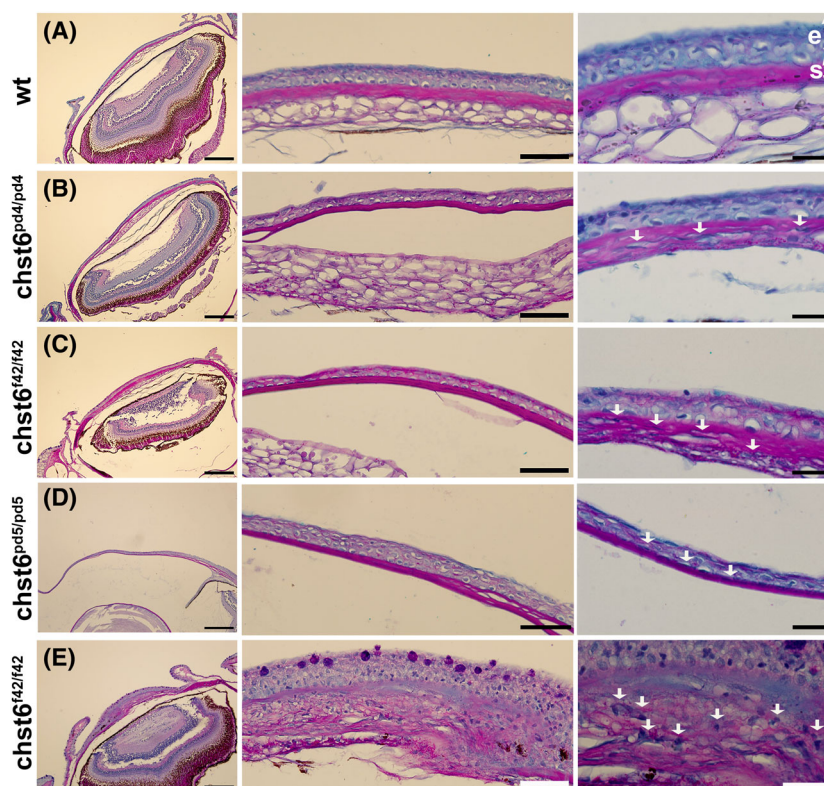


Fig. 7. Histopathology of the corneal tissue in the mutant zebrafish. Alcian blue/periodic acid–Schiff-stained eye sections of (A) wt, (B) *chst6*^{pd4/pd4}, (C) *chst6*^{f42/f42}, (D) *chst6*^{pd5/pd5}, and (E) *chst6*^{f42/f42} are shown ($n = 7$). Left column: 10 \times overview, scale bars: 200 μ m; middle column: 40 \times close-up overview, scale bars: 50 μ m; right column: 100 \times zoom, scale bars: 20 μ m. Serial sections were taken from each eye, and different slices were shown in the middle and right columns. Collagen in stroma is stained pink with periodic acid–Schiff, mucopolysaccharides are stained blue with alcian blue, and nucleus is stained light purple with hematoxylin. e, epithelium; s, stroma. White arrows indicate alcian blue-positive aggregates.

(Fig. 7B). Some mutants had degenerated posterior stroma and Descemet's membrane and blue deposits on this level (Fig. 7C). Although the stroma was thinner in most mutants, some lost stroma almost completely (Fig. 7D), one very old mutant (30 mpf) carrying the *chst6*^{f42/f42} allele had atypical cornea structure, which has an overgrown and irregular epithelium and very thick cornea (Fig. 7E).

Another characteristic of MCD is loss of cKS in the corneal stroma. While cKS was present in the corneal stroma of wt zebrafish, it was completely lost in all homozygous mutants (Fig. 8A–D). TGF-beta induced protein (BIGH3) is an epithelial marker in the human cornea. BIGH3 was present in the epithelium and at low levels in the stroma of zebrafish adult eye of wt fish. In the mutants, BIGH3 expression in the corneal epithelium was not affected, whereas it was lost in the stroma of *chst6*^{pd4/pd4}, *chst6*^{pd5/pd5}, and decreased in the stroma of *chst6*^{f42/f42} homozygous mutants (Fig. 8E–H). The thickness of the cornea was

measured in cryosections and found to be decreased in all mutants (Fig. 8I,J).

Discussion

Macular corneal dystrophy patients were reported to have different mutations causing enzyme loss-of-function. Conservation among species and frequency of mutagenesis for each residue was reported [27]. Density of the mutations was highest between 46 and 77. aa, with 25 out 32 residues mutated in multiple patients, and 23 of these mutated residues are identical in zebrafish CHST6 protein [27]. By analyzing the homology model of CHST6 protein, we showed that R53 located in 1st PAPS domain binds the sulfate donor, hence is most likely to be the enzyme active site. We also confirmed the accuracy of our modeled structure with later published AlphaFold predicted model (AF-Q9GZX3-F1). Inactivation of 1st PAPS by introduction of an indel via gRNA1 or a deletion via

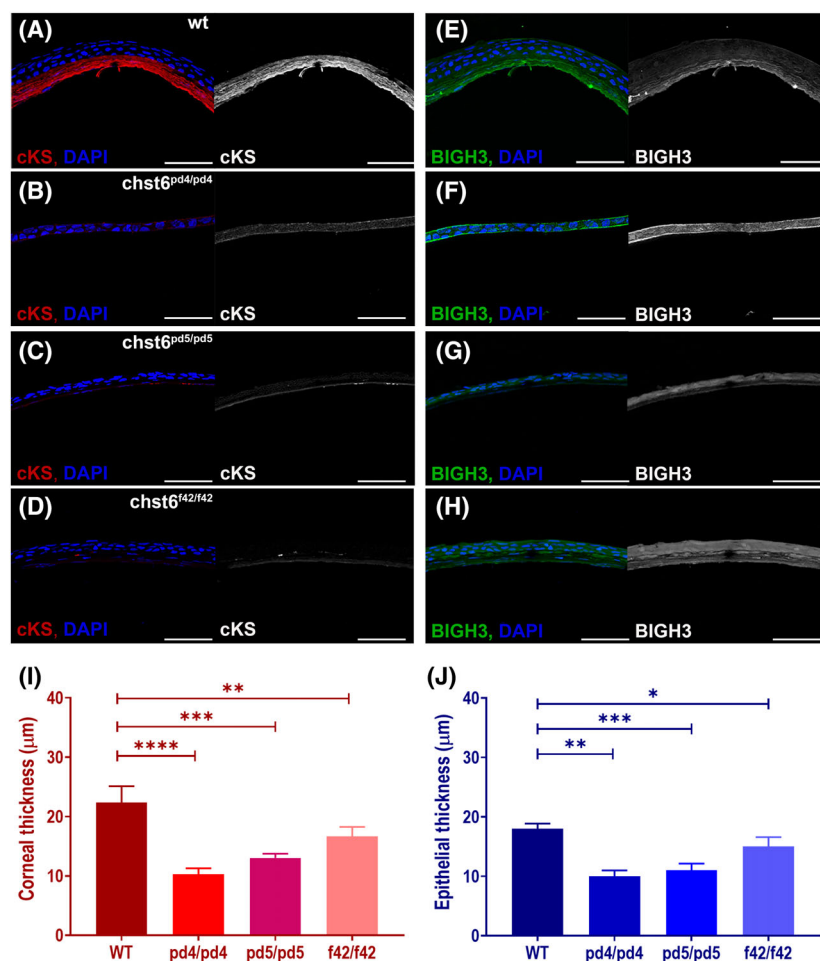


Fig. 8. Corneal keratan sulfate (cKS) is reduced and BIGH3 expression is altered in the cornea of the adult mutant fish. Corneal sections stained with anti-cKS, anti-BIGH3, and DAPI are shown. (A) cKS (red) is detected in the corneal stroma of wt, but not detected in the mutant cornea as seen in images of (B) *chst6*^{pd4/pd4}, (C) *chst6*^{pd5/pd5}, (D) *chst6*^{f42/f42} mutant eye sections. Grayscale images of cKS signal are shown next to the overlay image; anti-cKS (red), DAPI (blue). (E) A strong stromal and weak epithelial BIGH3 (green) signal is detected in the cornea of the wt fish. BIGH3 is detected only in the epithelium of (F) *chst6*^{pd4/pd4} and (G) *chst6*^{pd5/pd5} mutants and (H) epithelium and stroma layers of the *chst6*^{f42/f42} mutant cornea. Scale bars: 80 μm. (I) Thickness of cornea ($n = 5$) and (J) corneal epithelium was measured from IF-stained cryosections represented in A–H ($n = 5$). Multiple t -test was used for the statistical analysis. Data are presented as the mean \pm std. $P < 0.05$ (*), $P < 0.01$ (**), $P < 0.001$ (***), and $P < 0.0001$ (****) vs the wt group.

gRNA1 and gRNA2 targeted CAS9 both resulted in successful mutagenesis and generation of loss-of-function mutants. Our attempts to generate mutants with deletion of the entire coding sequence were not successful. Even though the designed gRNA5 had the highest score according to specific algorithms that was developed based on empiric data, the deletion did not occur at the 5th a.a. as predicted. Instead, a fairly large deletion that started from 89th a.a. was generated, suggesting that either the DSB was not possible at this locus or it was repaired. The dynamics of Cas9 catalytic activity has been shown to vary at different target sites, and the chromosome openness at the target is proposed to be a factor, which may be the case here [29,30]. The fact that only heterozygous zebrafish were obtained with the large *chst6* deletion may indicate a vital role for integral *chst6* genomic region for survival.

Loss of function in the *chst6* mutants was proven by loss of enzyme activity as measured via the 5D4 cKS antibody. Quantification with ELISA showed that the

amount of cKS was decreased strongly in whole body of mutant larvae but did not completely disappear. In the zebrafish, genome *chst2* and *chst6* are the only genes encoding keratan sulfate N-acetylated glucosamine sulfotransferases. Although neither of these two genes were studied in depth, *chst2* expression was reported in the central nervous system [31]. The remaining cKS may be due to the activity of *chst2a* and/or *chst2b* genes. Immunofluorescence staining showed that corneal localized sulfated keratan sulfate signal was lost in the mutant larvae, and this was rescued when wt mRNA was injected to 1-cell stage embryos. Similarly, in adult zebrafish stromal cKS signal was completely lost in homozygous *chst6* mutants. The cKS loss was detected as of 4 dpf in all mutant zebrafish lines in all generations, which indicates that cKS loss precedes the vision loss.

In humans, *chst6* is predominantly present in cornea, whereas *chst5* takes on the same function in the intestine. We showed that *chst6* expression is initially ubiquitous in 24–30 hpf embryos, whereas it becomes

restricted to the head region by 72 hpf. Expression in the eye and cornea was detected at 72 hpf, which corresponds to a stage of corneal layer specification in zebrafish eye [19]. In parallel to the expression of *chst6* in the head and cornea, sulfated keratan sulfate was detected in these tissues of 4 dpf wt zebrafish and lost in the *chst6* mutants. These findings suggest that zebrafish *chst6* gene gained additional functions outside of cornea. Supporting this, a small portion of mutant embryos were malformed and did not survive. The morphological defects were seen in all alleles generated, and detailed report was deposited [32]. Both the cKS expression and morphological defects were rescued with wt mRNA injection which proves that the phenotypes are specifically due to *chst6* inhibition. The low penetrance of morphological defects among the mutants and presence of variable phenotypes indicates a complex regulatory mechanism. Keratan sulfate proteoglycans and all proteoglycans have tremendous diversity in structure due to not only the core proteins but also the diversity of disaccharide chain length and degree of sulfation. They have complex roles including regulation of the ECM stiffness and chemokine diffusion in the ECM, but also interact with various proteins and regulate their activities in health and disease [33,34]. Therefore, the low penetrance and variable phenotypes seen in *chst6* mutant zebrafish can be a result of an interplay between several factors which is beyond the scope of this manuscript and the mechanisms will be explored in future.

Some MCD patients also display loss of cKS in the serum indicating a systemic effect which is not yet understood completely [35]. Indeed, there are three variants of MCD in humans, characterized by immunophenotype. Type 1 patients have no detectable keratan sulfate in either the serum or cornea. In type 1A patients, keratan sulfate is absent in the serum but stroma shows immunoreactivity to keratan sulfate antibodies, whereas in MCD type 2, normal amounts of keratan sulfate are detected in the serum and stroma [36]. The source of serum cKS is not directly proven, since the antibody is specific to the sulfated form of Gal-GlcNAc but does not discriminate between different core proteins of KSPGs. The serum cKS is thought to be result of cKS breakdown in the cartilage and earlier reports showed loss of cKS in the cartilage tissues of MCD patients albeit with no clinical manifestations [11,12,37]. Since it was previously shown that cKS epitopes are expressed in the jaw cartilage of zebrafish larvae at 8 dpf, we explored the structure of jaw cartilage in mutants. We found an enlargement of the angle between to ceratohyal cartilages, and an increase of distance between the

Meckel's cartilage and ceratohyal joint in a small proportion of the mutants. This is in parallel to the low penetrance of gross morphological defects. Interestingly, allele f42 induced more significant change in the jaw phenotypes in larvae, and when these fish were raised to adulthood, some of them developed a prominent protruding mouth phenotype with both upper and lower lips being extended to front. Other mutants had open mouth phenotypes. Even though the healthy-looking larvae were selected at 5 dpf and raised to adulthood, some fish developed tail and body shape deformations over time and some adults had minor/major defects mainly at the posterior end. The last few vertebrae appeared stacked closer, and junctions were not properly spaced. In severe cases, posterior end was truncated and the caudal fin did not form. The defects in the vertebrae are reminiscent of skeletal defects reported in patients with mucopolysaccharidosis IVA disease in which KSPG accumulation is observed due to a defect in KSPG breakdown [38].

In the zebrafish MCD model described here, different mutant alleles were characterized through different generations and loss of keratan sulfate sulfation, and formation of opaque aggregates in the cornea was consistently observed. Formation of opaque aggregates in the eye occurred in adulthood as early as 8 months postfertilization, and incidence of opacity increased as the fish became 14 months or older. cKS signal in the corneal stroma was completely lost, and the alcian blue deposits were detected in both the corneal epithelium and stroma of the mutant zebrafish. Moreover, the thickness of cornea was reduced in mutants, and more pronounced thinning was detected in the epithelium. These structural changes in zebrafish cornea reflect the MCD patient symptoms well. In humans, the corneal deposits are not present at birth, but become visible in the 1st decade or around adolescence. The grayish white punctate opacities merge into larger areas over time, causing the entire corneal stroma to become cloudy. The corneal stroma between the deposits is also hazy, so that the vision is disturbed and necessitates corneal transplantation around 3rd–4th decades [39].

Few aspects of MCD in zebrafish differ from that of human. In zebrafish MCD, females developed opacities earlier than males; however, no gender predilection was reported in humans. *BIGH3* was found to be expressed in the corneal stroma of wt adult zebrafish, whereas in humans, it is solely epithelial [19]. Interestingly, *BIGH3* expression was lost or decreased in the stroma of *chst6* homozygous mutants. In humans, mutations in the *BIGH3* gene encoding for keratopithelin protein have been described in different corneal dystrophies such as granular corneal dystrophy,

lattice corneal dystrophy, and their different clinical subtypes, but not the MCD [40]. Yet, a link between KSPGs and TGF β is proposed by several studies. Induction of TGF β by lumican was shown in a joint fibrosis model [41]. Moreover, an interaction between lumican and TGF β pathway was reported in tumor progression and STRING database shows a direct interaction between lumican and TGF β I [42,43]. Our finding in zebrafish cornea also indicates a close relationship between KSPGs and TGF β I (BIGH3) distribution in the ECM of zebrafish, which is a concept to be explored further.

In conclusion, an *in vivo* zebrafish model of MCD was developed by CRISPR/Cas9-mediated mutagenesis of *chst6* gene. To our knowledge, this is the first report of an MCD animal model and first study showing that zebrafish cornea can be used to model stromal corneal dystrophies. The zebrafish *chst6* mutants also showed skeletal defects shedding light on the poorly understood roles of KSPG sulfation in the skeletal tissues. Patient symptoms and structural changes in the MCD cornea were well reproduced in the zebrafish model which paves the way to use this as a preclinical test model.

Methods

Zebrafish maintenance

Zebrafish were reared under standard conditions in Izmir Biomedicine and Genome Center (IBG) Zebrafish Facility. Wild-type AB strain was used to generate the mutant lines. All experiments were approved by the IBG local ethics committee (IBG-HADYEK) with protocols number 202323 and 21/2019. Homozygous mutants were outcrossed to wt to clean the background and avoid inbreeding. The crossing schemes are reported in the Results section.

In situ hybridization and rescue experiment

Whole mount *in situ* hybridization was done as published before [44]. The coding sequence of *chst6* was amplified with forward 5' ATCGTGCTCGAGATGGCAA 3', reverse 5' AATGCACAAATGCCCCAGAA 3' primers and cloned into pGEM-T vector (#A3600; Promega, Madison, WI, USA). A full-length antisense probe was synthesized from this plasmid. A short probe was synthesized from a PCR product generated with forward 5' ATGCTGCGCTGGAGAGTGT 3' and reverse 5' TAATACGACTCACTAGAGGAATGCACAAATGCCCCAGAA 3' primers. The probes were transcribed with TranscriptAid T7 High Yield Transcription kit (#KO441; Thermo Scientific, Waltham, MA, USA) using DIG RNA Labeling Mix (#11277073910; Roche, Basel, Switzerland). For the rescue experiment, the *chst6* coding sequence was subcloned into pCS2 plasmid

and linearized with NotI and mRNA was synthesized with mMESSAGE mMACHINE™ SP6 Transcription Kit (#AM1340; Invitrogen, Carlsbad, CA, USA). mRNA (400 ng· μ L⁻¹) was injected into the zygotes.

Generation of mutants with CRISPR/Cas9

Guide RNA (gRNA) sequences were designed with the CRISPRscan web tool, and gRNAs were synthesized according to published protocols [28,45]. Cas9 mRNA was synthesized from plasmids [28,46]. pCS2-nCas9n was a gift from W. Chen (Addgene plasmid #47929; <http://n2t.net/addgene:47929>; RRID: Addgene_47_929). pCS2-nCas9n-nanos 3'UTR was a gift from A. Giraldez (Addgene plasmid #62542; <http://n2t.net/addgene:62542>; RRID: Addgene_62_542). Injection mix was prepared with 250 ng· μ L⁻¹ of Cas9 mRNA, 50 ng· μ L⁻¹ of each gRNA, 0.005% phenol red in RNase-free ultrapure water, and delivered to the embryo at one-cell stage. nCas9n-nanos UTR was used for gRNA3 and gRNA5 injections to reduce lethality.

Verification of mutagenesis and genotyping

For genotyping, DNA lysates of fin clips from individual fish, single or pooled embryos (up to 8) were prepared as described previously [47]. A 522 bp portion of the genomic DNA was amplified with forward 1: 5' CCACTGCTAA TGTCGTGATGTT 3' and reverse 1: 3' CGCAGTGCTTT TTGCAGTCT 5' primers, for genotyping. Deletion mutations were identified by shift of mobility on agarose gel. Small indel mutations were identified by the T7 Endonuclease I (#MO302L; New England Biolabs, Ipswich, MA, USA) mismatch assay, according to the product manual. A 1.3 kb portion of genomic DNA was amplified with forward 1: 5' CCACTGCTAATGTCGTGATGTT 3' and reverse 2: 3' CGCAGTGCTTT-TTGCAGTCT 5' primers for Sanger sequencing. Primers were designed with the SNAPGENE software version 5.2.5.1 (GSL Biotech LLC., Boston, MA, USA). The sequence alignment was performed with the CLUSTAL OMEGA (EMBL-EBI, Hinxton, UK) software.

Quantification of cKS with ELISA

Five days postfertilization larvae were collected and snap-frozen with liquid nitrogen. Frozen larval pellet (50 larvae) was crushed manually with a micro pestle, in 50 μ L PBS that contains 1 μ L protease inhibitor cocktail (#ab201111; Abcam, Cambridge, MA, USA). Tissue debris was removed with centrifugation at 13 800 g, 4 °C for 5 min. Total protein was calculated by the bicinchoninic acid assay (#23227; Thermo Fisher Scientific, Waltham, MA, USA). Fifty microliter of standard, blank, and samples were loaded into the antibody-coated wells. ELISA was performed using the kit manufacturer's (#MBS288502; MyBioSource, San Diego, CA, USA) protocol. Fifty larvae

per replica of each group were used, and average of three replica was calculated. The standard graph was plotted with the nonlinear 4-parameter sigmoidal curve method, and the concentration of samples was calculated using the EXCEL (Microsoft, Redmond, WA, USA) software.

Whole mount alcian blue staining

The larvae were fixed with 4% paraformaldehyde (PFA) O/N, at 4 °C. The larvae were dehydrated by passing through 25% – 50% – 75% and 100% ethanol series prepared in PBS with 0.1% Tween. 1 mg·mL⁻¹ alcian blue (#ab145250; Abcam Limited, Cambridge, UK) working solution was prepared in 70/30 (v/v) ethanol/glacial acetic acid (GAA) mixture. Larvae were kept in the alcian blue working solution for O/N at room temperature. The samples were washed with 100% GAA 2 times for 30 min each, to stop the staining. Transfer to ethanol was done by immersing in 70/30 (v/v), 30/70 (v/v) GAA/ethanol, and 100% ethanol for 30 min each. Rehydration was done with 5 min washes in 75% – 50% – 25% – 0% ethanol in PBS. Bleaching solution (0.5% KOH, 3% H₂O₂ in water) was applied until the eyes became yellowish. The samples were washed three times with PBS and treated with 1% trypsin/PBS (#T1426; Sigma Aldrich, Burlington, MA, USA) until the background was cleared. Samples were washed thoroughly with PBS and mounted as whole or dissected for imaging. Imaging was done with SZX10 stereomicroscope and CKX41 compound microscope (Olympus, Tokyo, Japan).

Statistical analysis

Statistical analyses were performed using the GRAPHPAD PRISM 10.0 (GraphPad Software, Boston, MA, USA). Normal distributions of the groups were assessed using the Shapiro–Wilk and D'Agostino–Pearson tests. The unpaired *t*-test was used for groups with normal distribution, while the Mann–Whitney *U* test was used for groups with abnormal distribution.

Immunofluorescence staining

The larvae were fixed with 4% PFA for overnight at 4 °C, washed with PBS and then dehydrated with 25% – 50% – 75% – 100% methanol, and kept in 100% methanol at –20 °C for up to 24 h. The larvae were transferred to PBS and washed with 1× PDT (PBS, 0.1% Tween-20, 0.3% Triton-X, 1% DMSO), two times for 30 min each. Then, samples were incubated for 1 h at 37 °C with 10 µg·µL⁻¹ proteinase K (#P-480; Gold Biotechnology, St. Louis, MO, USA) or 0.5 U·mL⁻¹ chondroitinase (#C3667; Thermo Fisher Scientific, Waltham, MA, USA). Chondroitinase treatment was necessary for the cKS stainings of the zebrafish larvae. Standard staining protocol was used as published before [48]. Immunofluorescence staining of adult cornea was

performed on cryosections. One eye of euthanized zebrafish was surgically removed and fixed in %4 formaldehyde and O/N at room temperature, and rest of the fish body was used for paraffin embedding. Fixed eye tissue was rinsed with PBS and immersed in 30% sucrose for 3 days at 4 °C until eyes sank to the bottom of the tube. Next, tissue was transferred into OCT (#4583; Sakura, Torrance, CA, USA) and kept at –20 °C for 30 min and –80 °C O/N. Fourteen micrometer sections were taken with a cryostat (#CM 1950; Leica, Buffalo Grove, IL, USA) and transferred onto slides (#J1800AMNZ; Eprexia, Portsmouth, NH, USA). Slides were stored at –80 °C, until further processing. Immunofluorescence staining slides were done as described previously [49]. 5D4 anti-keratan sulfate (#MAB2022, 1 : 200; Millipore, Burlington, MA, USA), BIG-H3 (#2719S, 1 : 200; Cell Signaling Technology, Danvers, MA, USA) and goat anti-mouse, Alexa Fluor 594 (#8890S, 1 : 400; Cell Signaling Technology, Danvers, MA, USA), and goat anti-mouse Alexa Fluor 488 (#4408S, 1 : 400; Cell Signaling Technology) were used as primary and secondary antibodies.

Histopathology

Euthanized zebrafish were fixed in 10% neutral buffered formalin (NBF, #HT501128; Sigma Aldrich, Burlington, MA, USA) for at least 6 days. Following fixation, the fish were treated with a 0.35 M EDTA/PBS solution for 5 days to soften the bones. Tissue was passed through ethanol series (70%, 80%, 96%, 100%, 100%) to dehydrate. Samples were incubated in fresh xylene (#1082972500; Merck, Darmstadt, Germany) two times for 45 min, paraffin for 1 h at 65 °C. After processing, whole body or heads were embedded in paraffin using a base mold. Blocks were frozen at –20 °C for at least 3 h. Five micrometer thick sections were placed on poly-L-lysine-coated slides (#ANT-MS90PS01W; Laborant, Istanbul, Turkey). Alcian blue/periodic acid–Schiff staining (#04-163802; Bio-Optica, Milan, Italy) was performed according to the manufacturer protocol.

Imaging of adult eye

Adult zebrafish were anesthetized using 0.04% ethyl 3-aminobenzoate methanesulfonate salt (#A5040; Supelco, Bellefonte, PA, USA). The zebrafish eyes were imaged with an Olympus SZX10 stereomicroscope with 4× magnification, with top illumination. After examination, the fish were promptly returned to the system water. Procedure was repeated every 2 months.

Vision test with adult fish

Wild-type and mutant adult fish in their rearing tanks were kept in equal numbers, and time for adjustment to environment was given to fish before food was dispersed. Video recordings were taken 1 min before and after feeding. The

second in which the feed was dispersed was considered time zero. The time it takes for the fish to reach the food was recorded, and the path of each fish to reach the food was tracked with AVIDEMUX software (<https://avidemux.sourceforge.net/>).

Acknowledgements

This study was funded by TUBITAK Grant no. 219S943. Additionally, EE-G and HO were supported by TUBITAK-BIDEB; MB was supported by Abdi Ibrahim Foundation scholarships. We thank undergraduate interns Rabia Altintas, Serhat Songören and Ege Seray Ceyhan for their contributions to early phases of this work. Authors thank Izmir Biomedicine and Genome Center Zebrafish Facility, Histopathology Core Facility and Optical Imaging Core Facility, for supporting the experiments. Authors extend gratitude to Serif Senturk for helpful discussions regarding the CRISPR/Cas9 method and for being the academic advisor of MB. Authors thank Emine Gelinci for fish care and Emine Gelinci and Ece Uzun for their excellent help with histopathology procedures. Authors are grateful to Ozge Bahar Akdogan for illustration of the graphical abstract.

Conflict of interest

The authors declare no conflict of interest. The disease model reported here is filed for patenting PCT/TR2023/051790.

Author contributions

MB and EE-G performed experiments, analyzed data, wrote results, and prepared figures. HO performed experiments and analyzed data. SK modeled protein structure and contributed to project planning. CAU contributed to project planning and evaluation of results. GC-A conceived the project, acquired funding, performed experiments, supervised the work, and wrote the manuscript.

Peer review

The peer review history for this article is available at <https://www.webofscience.com/api/gateway/wos/peer-review/10.1111/febs.17337>.

Data availability statement

The data that support the findings of this study are available in the figures, tables, and [Supporting Information](#) of this article.

References

- Hassell JR & Birk DE (2010) The molecular basis of corneal transparency. *Exp Eye Res* **91**, 326–335.
- Akhtar S, Alkatan HM, Kirat O, Khan AA & Almubrad T (2015) Collagen fibrils and proteoglycans of macular dystrophy cornea: ultrastructure and 3D transmission electron tomography. *Microsc Microanal* **21**, 666–679.
- Lewis PN, Pinali C, Young RD, Meek KM, Quantock AJ & Knupp C (2010) Structural interactions between collagen and proteoglycans are elucidated by three-dimensional electron tomography of bovine cornea. *Structure* **18**, 239–245.
- Lindahl U, Couchman J, Kimata K & Esko JD (2017) Chapter 17: Proteoglycans and sulfated glycosaminoglycans. In *Essentials of Glycobiology* (Varki A, Cummings RD, Esko JD, *et al.*, eds), 3rd edn, Cold Spring Harbor Laboratory Press, Cold Spring Harbor, NY. <https://www.ncbi.nlm.nih.gov/books/NBK453033/>; 10.1101/glycobiology.3e.017
- Caterson B & Melrose J (2018) Keratan sulfate, a complex glycosaminoglycan with unique functional capability. *Glycobiology* **28**, 182–206.
- Pellegata NS, Dieguez-Lucena JL, Joensuu T, Lau S, Montgomery KT, Krahe R, Kivela T, Kucherlapati R, Forsius H & de la Chapelle A (2000) Mutations in KERA, encoding keratocan, cause cornea plana. *Nat Genet* **25**, 91–95.
- Niel F, Ellies P, Dighiero P, Soria J, Sabbagh C, San C, Renard G, Delpech M & Valleix S (2003) Truncating mutations in the carbohydrate sulfotransferase 6 gene (CHST6) result in macular corneal dystrophy. *Invest Ophthalmol Vis Sci* **44**, 2949–2953.
- Klinterworth GK & Smith CF (1977) Macular corneal dystrophy. *Am J Pathol* **89**, 167–182.
- Funderburgh JL (2002) Keratan sulfate biosynthesis. *IUBMB Life* **54**, 187–194.
- Saito T, Nishida K, Nakayama J, Akama TO, Fukuda MN, Watanabe K, Quantock AJ, Maeda N, Watanabe H & Tano Y (2008) Sulfation patterns of keratan sulfate in different macular corneal dystrophy immunophenotypes using three different probes. *Br J Ophthalmol* **92**, 1434–1436.
- Plaas AH, West LA, Thonar EJ, Karcioğlu ZA, Smith CJ, Klinterworth GK & Hascall VC (2001) Altered fine structures of corneal and skeletal keratan sulfate and chondroitin/dermatan sulfate in macular corneal dystrophy. *J Biol Chem* **276**, 39788–39796.
- Thonar EJ-MA, Lenz MKG, Klinterworth GK, Caterson B, Pachman LM, Gluckman P, Katz R, Huff J & Kuettner KE (1985) Quantification of keratan sulfate in blood as a marker of cartilage catabolism. *Arthritis Rheum* **28**, 1367–1376.

- 13 Thonar EJ & Glant T (1992) Serum keratan sulfate a marker of predisposition to polyarticular osteoarthritis. *Clin Biochem* **25**, 175–180.
- 14 Edward DP, Thonar EJ-MA, Srinivasan M, Yue BJYT & Tso MOM (1990) Macular dystrophy of the cornea a systemic disorder of keratan sulfate metabolism. *Ophthalmology* **97**, 1194–1200.
- 15 Palka BP, Sotozono C, Tanioka H, Akama TO, Yagi N, Boote C, Young RD, Meek KM, Kinoshita S & Quantock AJ (2010) Structural collagen alterations in macular corneal dystrophy occur mainly in the posterior stroma. *Curr Eye Res* **35**, 580–586.
- 16 Kaya SG, Inanc-Surer S, Cakan-Akdogan G, Oktay G, Utine CA & Kalyoncu S (2021) Roles of matrix metalloproteinases in the cornea: a special focus on macular corneal dystrophy. *Med Drug Discov* **11**, 100095.
- 17 Murab S, Chameettachal S & Ghosh S (2016) Establishment of an in vitro monolayer model of macular corneal dystrophy. *Lab Invest* **96**, 1311–1326.
- 18 Hayashida YAT, Beecher N, Lewis P, Young RD, Meek KM, Kerr B, Hughes CE, Caterson B, Tanigami A, Nakayama J *et al.* (2006) Matrix morphogenesis in cornea is mediated by the modification of keratan sulfate by GlcNAc 6-O-sulfotransferase. *Proc Natl Acad Sci USA* **36**, 13333–13338.
- 19 Zhao XC, Yee RW, Norcom E, Burgess H, Avanesov AS, Barrish JP & Malicki J (2006) The zebrafish cornea: structure and development. *Invest Ophthalmol Vis Sci* **47**, 4341–4348.
- 20 Puzzolo D, Pisani A, Malta C, Santoro G, Meduri A, Abbate F, Montalbano G, Wylegala E, Rana RA, Bucchieri F *et al.* (2018) Structural, ultrastructural, and morphometric study of the zebrafish ocular surface: a model for human corneal diseases? *Curr Eye Res* **43**, 175–185.
- 21 Souza AR, Kozlowski EO, Cerqueira VR, Castelo-Branco MT, Costa ML & Pavao MS (2007) Chondroitin sulfate and keratan sulfate are the major glycosaminoglycans present in the adult zebrafish *Danio rerio* (Chordata-Cyprinidae). *Glycoconj J* **24**, 521–530.
- 22 Yeh LK, Liu CY, Chien CL, Converse RL, Kao WW, Chen MS, Hu FR, Hsieh FJ & Wang IJ (2008) Molecular analysis and characterization of zebrafish keratocan (zKera) gene. *J Biol Chem* **283**, 506–517.
- 23 Yeh LK, Liu CY, Kao WW, Huang CJ, Hu FR, Chien CL & Wang IJ (2010) Knockdown of zebrafish lumican gene (zlum) causes scleral thinning and increased size of scleral coats. *J Biol Chem* **285**, 28141–28155.
- 24 Thisse B & Thisse C (2004) Fast Release Clones: A High Throughput Expression Analysis. ZFIN Direct Data Submission.
- 25 Hayes AJ, Mitchell RE, Bashford A, Reynolds S, Caterson B & Hammond CL (2013) Expression of glycosaminoglycan epitopes during zebrafish skeletogenesis. *Dev Dyn* **242**, 778–789.
- 26 Ersoz-Gulseven E, Basol M, Özaktaş H, Kalyoncu S, Utine CA & Cakan-Akdogan G (2024) Zebrafish carbohydrate sulfotransferase 6 (chst6) mutants provide a preclinical model for macular corneal dystrophy. *bioRxiv*. doi: [10.1101/2024.01.24.577150](https://doi.org/10.1101/2024.01.24.577150)
- 27 Zhang J, Wu D, Li Y, Fan Y, Dai Y & Xu J (2019) A comprehensive evaluation of 181 reported CHST6 variants in patients with macular corneal dystrophy. *Aging* **11**, 1019–1029.
- 28 Moreno-Mateos MA, Vejnar CE, Beaudoin JD, Fernandez JP, Mis EK, Khokha MK & Giraldez AJ (2015) CRISPRscan: designing highly efficient sgRNAs for CRISPR-Cas9 targeting in vivo. *Nat Methods* **12**, 982–988.
- 29 Kuscü C, Arslan S, Singh R, Thorpe J & Adli M (2014) Genome-wide analysis reveals characteristics of off-target sites bound by the Cas9 endonuclease. *Nat Biotechnol* **32**, 677–683.
- 30 Kraft K, Geuer S, Will AJ, Chan WL, Paliou C, Borschiwer M, Harabula I, Wittler L, Franke M, Ibrahim DM *et al.* (2015) Deletions, inversions, duplications: engineering of structural variants using CRISPR/Cas in mice. *Cell Rep* **10**, 833–839.
- 31 Rauch GJ, Lyons DA, Middendorf I, Friedlander B, Arana N, Reyes T & Talbot WS (2003) Submission and Curation of Gene Expression Data. ZFIN. <http://zfin.org>
- 32 Basol M (2022) *Generation of CHST6 zebrafish mutants via CRISPR/CAS9 system, and phenotypic analysis of mutants*. Dokuz Eylül University, İzmir, Türkiye.
- 33 Carlson EC, Sun Y, Auletta J, Kao WW, Liu CY, Perez VL & Pearlman E (2010) Regulation of corneal inflammation by neutrophil-dependent cleavage of keratan sulfate proteoglycans as a model for breakdown of the chemokine gradient. *J Leukoc Biol* **88**, 517–522.
- 34 Soares da Costa D, Reis RL & Pashkuleva I (2017) Sulfation of glycosaminoglycans and its implications in human health and disorders. *Annu Rev Biomed Eng* **19**, 1–26.
- 35 Klintworth GK, Meyer R, Dennis R, Hewitt AT, Stock EL, Lenz ME, Hassell JR, Stark WJ Jr, Kuettner KE & Thonar EJ (1986) Macular corneal dystrophy. Lack of keratan sulfate in serum and cornea. *Ophthalmic Paediatr Genet* **7**, 139–143.
- 36 Cursiefen C, Hofmann-Rummelt C, Schlotzer-Schrehardt U, Fischer DC, Haubeck HD, Kuchle M & Naumann GO (2001) Immunohistochemical classification of primary and recurrent macular corneal dystrophy in Germany: subclassification of

- immunophenotype IA using a novel keratan sulfate antibody. *Exp Eye Res* **73**, 593–600.
- 37 Wakitani S, Nawata M, Kawaguchi A, Okabe T, Takaoka K, Tsuchiya T, Nakaoka R, Masuda H & Miyazaki K (2007) Serum keratan sulfate is a promising marker of early articular cartilage breakdown. *Rheumatology (Oxford)* **46**, 1652–1656.
- 38 Khan S, Almeciga-Diaz CJ, Sawamoto K, Mackenzie WG, Theroux MC, Pizarro C, Mason RW, Orii T & Tomatsu S (2017) Mucopolysaccharidosis IVA and glycosaminoglycans. *Mol Genet Metab* **120**, 78–95.
- 39 Aggarwal S, Peck T, Golen J & Karcioğlu ZA (2018) Macular corneal dystrophy: a review. *Surv Ophthalmol* **63**, 609–617.
- 40 Sabir M (2020) The morphogenesis of granular and lattice corneal dystrophy – a mutation combination hypothesis. *Med Hypotheses* **145**, 110291.
- 41 Xiao D, Liang T, Zhuang Z, He R, Ren J, Jiang S, Zhu L, Wang K & Shi D (2020) Lumican promotes joint fibrosis through TGF- β signaling. *FEBS Open Bio* **10**, 2478–2488.
- 42 Brézillon S, Pietraszek K, Maquart FX & Wegrowski Y (2013) Lumican effects in the control of tumour progression and their links with metalloproteinases and integrins. *FEBS J* **280**, 2369–2381.
- 43 Szklarczyk D, Franceschini A, Wyder S, Forslund K, Heller D, Huerta-Cepas J, Simonovic M, Roth A, Santos A, Tsafou KP *et al.* (2015) STRING v10: protein-protein interaction networks, integrated over the tree of life. *Nucleic Acids Res* **43**, D447–D452.
- 44 Thisse C & Thisse B (2008) High-resolution in situ hybridization to whole-mount zebrafish embryos. *Nat Protoc* **3**, 59–69.
- 45 Vejnár CE, Moreno-Mateos MA, Cifuentes D, Bazzini AA & Giraldez AJ (2016) Optimized CRISPR-Cas9 system for genome editing in zebrafish. *Cold Spring Harb Protoc* **2016**, doi: [10.1101/pdb.prot086850](https://doi.org/10.1101/pdb.prot086850)
- 46 Jao LE, Wente SR & Chen W (2013) Efficient multiplex biallelic zebrafish genome editing using a CRISPR nuclease system. *Proc Natl Acad Sci USA* **110**, 13904–13909.
- 47 Samarut E, Lissouba A & Drapeau P (2016) A simplified method for identifying early CRISPR-induced indels in zebrafish embryos using high resolution melting analysis. *BMC Genomics* **17**, 547.
- 48 Sorrells S, Toruno C, Stewart RA & Jette C (2013) Analysis of apoptosis in zebrafish embryos by whole-mount immunofluorescence to detect activated caspase 3. *J Vis Exp* **82**, e51060.
- 49 Uribe RA & Gross JM (2007) Immunohistochemistry on cryosections from embryonic and adult zebrafish eyes. *CSH Protoc* **2007**, pdb.prot4779.

Supporting information

Additional supporting information may be found online in the Supporting Information section at the end of the article.

Video S1. Vision test video of three wild-type fish (age: 22 months) from Fig. 6H.

Video S2. Vision test video of three *chst6*^{pd4/pd4} fish (age: 23 months) from Fig. 6I.

Video S3. Vision test video of three *chst6*^{f42/f42} fish (age: 33 months) from Fig. 6J.